Coastal Engineering 88 (2014) 131–142

Contents lists available at ScienceDirect

Coastal Engineering

journal homepage: www.elsevier.com/locate/coastaleng

Laboratory study on wave dissipation by vegetation in combined current–wave flow

Zhan Hu [a,*], Tomohiro Suzuki [a,b], Tjerk Zitman [a], Wim Uittewaal [a], Marcel Stive [a]

[a] Dept. of Hydraulic Eng., Delft University of Technology, Stevinweg 1, 2628 CN Delft, The Netherlands
[b] Flanders Hydraulics Research, Berchemlei 115, 2140 Antwerp, Belgium

ARTICLE INFO

Article history:
Received 26 November 2013
Received in revised form 26 February 2014
Accepted 28 February 2014
Available online xxxx

Keywords:
Vegetation canopy
Wave dissipation
Current–wave flow
Drag force
Drag coefficient

ABSTRACT

Coastal wetlands such as salt marshes and mangroves provide valuable ecosystem services including coastal protection. Many studies have assessed the influence of plant traits and wave conditions on vegetation-induced wave dissipation, whereas the effect of tidal currents is often ignored. To our knowledge, only two studies investigated wave dissipation by vegetation with the presence of following currents (current velocity is in the same direction as wave propagation) (Li and Yan, 2007; Paul et al., 2012). However, based on independent experiments, they have drawn contradictive conclusions whether steady currents increase or decrease wave attenuation. We show in this paper that this inconsistency may be caused by a difference in ratio of imposed current velocity to amplitude of the horizontal wave orbital velocity. We found that following currents can either increase or decrease wave dissipation depending on the velocity ratio, which explains the seeming inconsistency in the two previous studies. Wave dissipation in plant canopies is closely related to vegetation drag coefficients. We apply a new approach to obtain the drag coefficients. This new method eliminates the potential errors that are often introduced by the commonly used method. More importantly, it is capable of obtaining the vegetation drag coefficient in combined current–wave flows, which is not possible for the commonly used calibration method. Based on laboratory data, we propose an empirical relation between drag coefficient and Reynolds number, which can be useful for numerical modeling. The characteristics of drag coefficient variation and in-canopy velocity dynamics are incorporated into an analytical model to help understand the effect of following currents on vegetation-induced wave dissipation.

1. Introduction

Coastal wetlands such as salt marshes and mangroves are important habitats for various plant and animal species. They also serve as buffers against erosive waves in coastal areas. The upstanding vegetation in coastal wetlands can significantly attenuate wave energy (Anderson et al., 2011), which can reduce the energy load on dikes and stabilize seabed (Callaghan et al., 2010; Shi et al., 2012). The possibility of integrating these natural habitats in coastal protection schemes has been subject of discussion (e.g. Borsje et al., 2011).

Previous laboratory and field measurements have shown that wave energy dissipation by vegetation (hereafter referred as WDV) is affected by both canopy traits and incident wave conditions (e.g. Bradley and Houser, 2009; Jadhav et al., 2013; Koftis et al., 2013; Möller, 2006; Yang et al., 2012; Ysebaert et al., 2011). It is generally agreed in the previous studies that a higher vegetation density, a lower submergence ratio (the ratio of water depth h to canopy height h_v) and stiffer plant stems lead to higher WDV (e.g. Bouma et al., 2005; Huang et al., 2011; Paul et al., 2012).

In most previous studies, the possible influence of background currents on WDV was not considered due to its complexity. However, it is often the case that when the tide penetrates the coastal wetlands during flooding phase, wind waves propagate in the same direction as the tidal currents. Using the waves as a reference, we designate such currents as following currents. The presence of following currents can affect the wave-damping capacity of vegetation. To our knowledge, Li and Yan (2007) and Paul et al. (2012) were the only two studies that conducted flume experiments and investigated the effect of following currents on WDV. Li and Yan (2007) concluded that following currents promoted WDV. They further demonstrated that WDV increased linearly with the velocity ratio α, defined as the ratio between imposed current velocity and amplitude of horizontal orbital velocity, i.e. U_c/U_w. Paul et al. (2012), on the other hand, found that tidal currents can strongly reduce the wave-damping capacity of their tested mimic canopies. The two studies gave contradicting conclusions about the effect of following currents on WDV. However, the α tested in the two studies was in a different range. The α tested in Li and Yan (2007) was 1.5–3.5, while in Paul et al. (2012) it was less than 0.5.

* Corresponding author. Tel.: +31 15 27 84846; fax: +31 15 27 85124.
E-mail address: zhan.hu@tudelft.nl (Z. Hu).

http://dx.doi.org/10.1016/j.coastaleng.2014.02.009
0378-3839/

Nevertheless, these two studies suggest that, firstly, the effect of a following current on WDV may depend on the α rather than on the magnitude of U_c alone and, secondly, it depends on α whether following currents enhance or suppress WDV. Therefore, systematic tests over a wide range of α are needed to properly identify the effect of following currents on WDV.

WDV is primarily induced by work done by drag force acting on the plant stems. A bulk drag coefficient (C_D) was introduced in previous modeling studies to account for the uncertainties lying in the plant-induced drag force F_D (e.g. Dalrymple et al., 1984; Mendez and Losada, 2004; Suzuki et al., 2011). Choosing C_D values is important to WDV prediction. However, the selection of C_D values for a natural vegetation meadow is challenging as it is affected by a number of factors. Specifically, C_D is closely related to the Reynolds number (Re), since it is profoundly influenced by the turbulence in canopies. Various empirical relations between C_D and Re have been proposed for vegetation in pure current or pure wave conditions (Nepf, 2011). Relations between C_D and the Keulegan–Carpenter number ($KC = U_w * T / b_v$, where T is the wave period and b_v is the plant stem diameter) have also been suggested in previous studies (Jadhav et al., 2013; Mendez and Losada, 2004). Moreover, the determination of C_D can be further complicated by the canopy stem density, plant morphology and stem stiffness (Nepf, 2011). Lastly, when a pure wave flow shifts to a combined current–wave flow, we expect that the C_D value varies accordingly. However, to our knowledge, the characteristics of vegetation drag coefficient in a combined current–wave flow have not yet been clarified.

In previous studies, C_D values for pure wave conditions have commonly been obtained by calibrating numerical models against observed WDV without measuring the actual force on plants (e.g. Bradley and Houser, 2009; Jadhav et al., 2013; Koftis et al., 2013; Mendez and Losada, 2004). In the case of a following current, this procedure may be inappropriate. The reason for this is that the existing models are intended to quantify WDV in pure wave conditions. As the effect of currents on WDV is not clear, the extension of these models to current–wave conditions may be invalid. Moreover, this method has two shortcomings. Firstly, the accuracy of the C_D values greatly depends on the quality of the model calibration against the measurements. The derived C_D value is unreliable when the correlation between the observations and modeling results is poor. Secondly, it is often assumed that the measured wave energy loss is solely induced by vegetation drag. Other dissipative processes, such as bed friction and wave breaking, are not explicitly considered but lumped into the vegetation drag, which can lead to an overestimated C_D.

Other than the calibration approach, C_D values can also be obtained via a more direct method. Infantes et al. (2011) measured the total force (F) and impact velocity on sea grass seedlings in pure current and pure wave conditions and derived C_D directly from the original Morison equation (Morison, 1950). They applied this method to compare the tolerance of different sea grass species to water motion. This direct method can help us to understand WDV processes by providing accurate C_D values that eliminate potential modeling errors. Furthermore, this method can be applied to plant canopies in combined current–wave flows since the Morison equation still holds in such conditions (Sumer and FredsØe, 2006; Zhou and Graham, 2000). This direct measuring method provides a way to obtain C_D values for vegetation in current–wave conditions, which is not possible for the commonly used calibration method.

Apart from the drag coefficient, insight in the flow structures inside the canopy is required for a proper understanding of WDV (Lowe et al., 2007). Compared to the extensive studies on unidirectional flow passing vegetated canopies, the flow structure for waves has been less studied (Lowe et al., 2005). In recent investigations a non-zero mean current velocity has been found in the vegetation canopies when the flow is driven purely by waves (Luhar et al., 2010; Pujol et al., 2013). The impact of this mean velocity on nutrient uptake and sediment transport has been identified, but its influence on WDV is not clear.

In this study, flume experiments with stiff plant mimics were carried out with a wide range of the ratio α to explore the effect of following currents on WDV. A direct force measurement method was applied to quantify C_D coefficients in both pure wave and current–wave flows. Vertical velocity profiles were also measured and the impact of a wave-induced mean current on WDV was illustrated. The insights of drag coefficients and velocity measurements were incorporated in an analytical model to explain the observed variation of WDV with α.

2. Methods

2.1. Flume setup

Experiments with plant mimics were conducted in a wave flume of the Fluid Mechanics Laboratory at Delft University of Technology. The wave flume is 40 m long and 0.8 m wide (schematized in Fig. 1a). A wave generator with an active wave absorption system is placed at one side of the flume (left in Fig. 1a). Imposed currents were in the same direction as the wave propagation. Hereafter, the direction of wave propagation is defined as '*positive*' and the opposing direction is defined as '*negative*'.

The mimic canopies were constructed by putting stiff wooden rods (Fig. 1d) in holes drilled in the false bottom (Fig. 1a). The height of the rods was 0.36 m and their diameter was 0.01 m. The canopy was 6 m long and 0.8 m wide and the stems were distributed uniformly in space. Three mimic stem densities (N), namely 62, 139 and 556 stems/m^2, were constructed by putting corresponding number of rods into the plates with drilled holes (Fig. 2). The three stem densities are denoted as VD1, VD2 and VD3, respectively. Control tests (VD0) were carried out with no mimic stems in the flume to measure the wave height reduction by the friction of flume bed and sidewalls. Two water depths were chosen to form emergent and submerged canopies. The water levels were at z = 0.25 m and z = 0.50 m respectively. The corresponding submergence ratios (h/h_v) were 1 and 1.39.

The force F on 4 individual stems in the mimic canopies was measured by 4 force transducers (Fig. 1a). These stems are identical to the ones in the mimic canopies. The bottom end of each these stems was attached to a force transducer by a screw which was fixed inside the stems (Fig. 1b). In the flume, the force transducers were mounted into the false bottom to avoid disturbance of the flow (Fig. 1b). The force transducers were developed by Delft Hydraulics (Delft, The Netherlands). Tests with known weights revealed that the voltage output of the transducers varies linearly with the force exerted on them with an estimated accuracy of 1%. In the tests, these forces ranged from −1.8 N to 1.8 N (where the sign refers to the direction of the force). This covers the working range of the transducers in the experiment (−0.3 N to 1.0 N). Data was sampled at 1000 Hz in order to capture the variation of F within a wave period (1 s–2.5 s). The force transducers had been used before in studies that compared the tolerance of seedlings to the drag force induced by currents or waves (Bouma et al., 2005; Infantes et al., 2011). A detailed description of the force transducers can be found in Bouma et al. (2005).

The instantaneous horizontal velocity (u) was measured by 4 EMFs (electromagnetic flow manufacture meters), which were made by Delft Hydraulics. Velocity (u) was measured at the same wave flume cross sections as the force transducers, to obtain the in-phase data (Fig. 1c). With

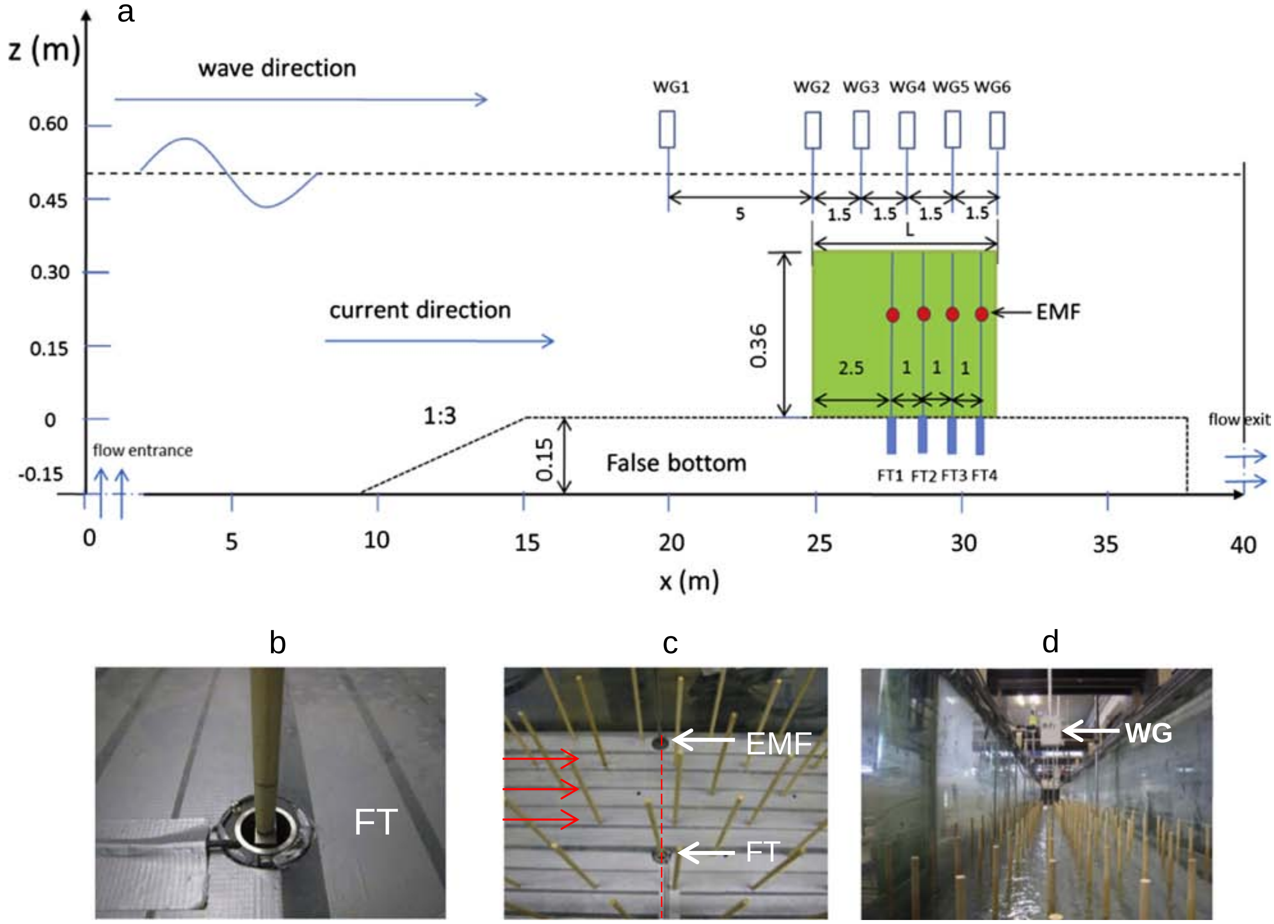

Fig. 1. Wave flume setup. (a) Schematic flume configuration and instrument deployment; (b) force transducer in the flume bed; (c) EMF and force transducer at the same cross section in the flume, the following current flows from the left to the right indicated by the three parallel arrows; (d) mimic plant canopy (low mimic stem density); WG1–WG6 stands for wave gauges, EMF stands for electromagnetic flow meter, FT1–FT4 stands for force transducers and L = 6 m is the length of the mimic plant canopy.

different water depths, u was measured at mid depth. To obtain velocity profiles, the EMF probes were moved vertically. In emergent canopy cases the velocity was measured at $z = 0.025$ m, 0.075 m, 0.125 m and 0.175 m. For submerged canopy cases, u was measured at $z = 0.05$ m, 0.15 m, 0.25 m, 0.30 m, 0.325 m, 0.375 m, 0.40 m and 0.45 m. Note that the measurement resolution was refined near the top of the canopy ($z = 0.36$ m). Six capacitance-type wave gauges made by Delft Hydraulics (WG1–WG6) were installed in the flume to measure the wave height (see Fig. 1a and d). WG1 was placed at $x = 20$ m, which was 5 m in front of the canopy. WG2–WG6 were placed 1.5 m apart from each other in the canopy, starting at $x = 25$ m. The output of EMF and WG was also in voltage, which can be converted to velocity and water level by linear regression relations. The accuracy of the EMFs and WGs was 1% and 0.5% respectively (Delft Hydraulics, 1990, year unknown).

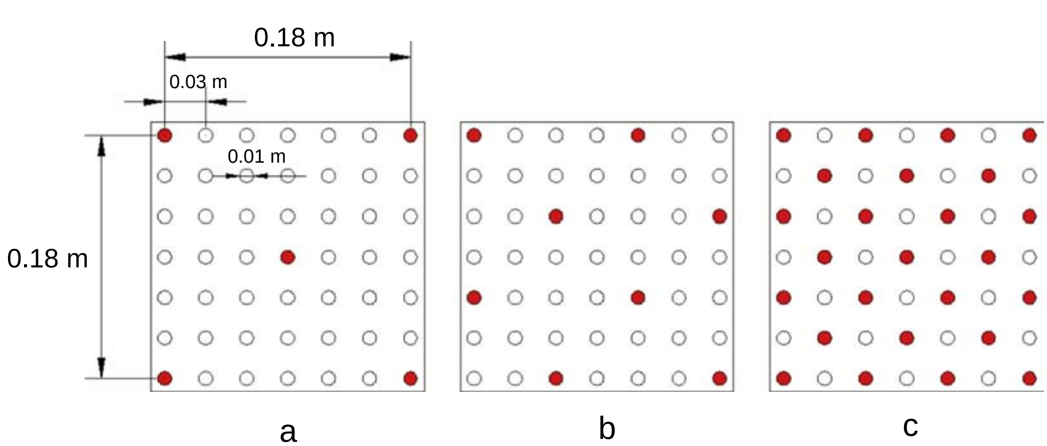

Fig. 2. Top view of the mimic plant canopy. (a) Low density (VD1); (b) medium density (VD2); (c) high density (VD3).

Table 1
Test conditions with different combinations of hydrodynamic conditions and mimic canopy configurations.

Source	Plant mimic type	Water depth (h)/ plant height [m]	Mimic stem density (N) [stems/m^2]	Wave height (H) [m]	Wave period (T) [s]	Wave case name	Current velocity (U_c) [m/s]
Present study	Stiff wooden rods	0.25/0.36	62/139/556	0.04	1.0	wave0410[a]	0/0.05/0.15/0.20
			62/139/556	0.04	1.2	wave0412	0/0.05/0.15/0.20
			62/139/556	0.06	1.0	wave0610	0/0.05/0.15/0.20
			62/139/556	0.06	1.2	wave0612	0/0.05/0.15/0.20
			62/139/556	0.08	1.2	wave0812	0/0.05/0.15/0.20
			62/139/556	0.08	1.5	wave0815	0/0.05/0.15/0.20
			62/139/556	0.10	1.5	wave1015	0/0.05/0.15/0.20
		0.50/0.36	62/139/556	0.04	1.0	wave0410	0/0.05/0.15/0.20/0.30
			62/139/556	0.06	1.2	wave0612	0/0.05/0.15/0.20/0.30
			62/139/556	0.08	1.4	wave0814	0/0.05/0.15/0.20/0.30
			62/139/556	0.10	1.6	wave1016	0/0.05/0.15/0.20/0.30
			62/139/556	0.12	1.6	wave1216	0/0.05/0.15/0.20/0.30
			62/139/556	0.12	1.8	wave1218	0/0.05/0.15/0.20/0.30
			62/139/556	0.15	1.6	wave1516	0/0.05/0.15/0.20/0.30
			62/139/556	0.15	1.8	wave1518	0/0.05/0.15/0.20/0.30
			62/139/556	0.15	2.0	wave1520	0/0.05/0.15/0.20/0.30
			62/139/556	0.18	2.2	wave1822	0/0.05/0.15/0.20/0.30
			62/139/556	0.20	2.5	wave2025	0/0.05/0.15/0.20/0.30
Li and Yan (2007)	Semi-rigid rubber rods	0.25/0.15	1111[b]	0.04/0.05/0.07	0.7/0.9/1.1	–	0.18/0.27/0.32
Paul et al. (2012)	Flexible poly ribbon	0.30/(0.15 & 0.30)	500/2000[c]	0.1	1	–	0/0.10

[a] The case name is created using a combination of incident wave height 0.04 m and wave period 1.0 s, namely wave0410.
[b] Mimic stem diameter tested in Li and Yan (2007) is 6–8 mm. Hence, the frontal area per canopy volume (N^*b_v as in Nepf, 2011) is 6.67 m^{-1}–8.89 m^{-1}, which is comparable to that of the VD3 tests (5.56 m^{-1}) in the present study.
[c] The width of the flexible mimics in the experiment was 0.2 cm. Hence, the frontal area per canopy volume in their test is 1.00 m^{-1} and 4.00 m^{-1} respectively, which is comparable to that of VD2 and VD3 tests (1.39 m^{-1} and 5.56 m^{-1} respectively) in the present study. The tests with stiff mimics in their test were excluded from comparison since their densities were not comparable to the present study.

In total, 314 tests were carried out with 3 different mimic stem densities, 2 water depths and various wave–current conditions (Table 1). The considered velocity ratio α was in the range of 0–5.4. For the emergent canopies, 7 different wave conditions were tested in combination with 4 steady current velocities (including the tests when $U_c = 0$ m/s). In the submerged canopies, 11 wave conditions were tested in combination with 5 steady current velocities. Hereafter, the subscript '*pw*' stands for pure wave conditions and subscript '*cw*' stands for combined current–wave conditions. It was noted that the wave height could be reduced when waves propagate in the same direction as current velocity due to the Doppler Effect (Demirbilek et al., 1996). To compensate for such loss, the incident wave height was amplified in current–wave cases to maintain the targeted wave height. The difference in wave height was less than 3% between the tests with different current velocities.

2.2. Data analysis

2.2.1. Velocity data analysis

The measured instantaneous horizontal flow velocity [m/s] can be expressed as:

$$u(t) = U_{mean} + U_w \sin(\omega t) + U' \tag{1}$$

where, ω is the wave angular frequency [Hz], t is time [s], U' stands for turbulent velocity fluctuations [m/s] and U_w is the amplitude of the horizontal wave orbital velocity [m/s], defined as

$$U_w = \frac{1}{2}(u_{\max} - u_{\min}) \tag{2}$$

where u_{max} and u_{min} are the peak flow velocities [m/s] in the positive and negative directions in a wave period, respectively. U_{mean} is the wave-averaged velocity [m/s] and can be defined as (e.g. Pujol et al., 2013):

$$U_{mean} = \frac{\omega}{2\pi} \int_{-\pi/\omega}^{\pi/\omega} u dt. \tag{3}$$

Note that U_{mean} is not equal to the imposed steady velocity U_c. The difference between the two is that U_{mean} is the period-averaged velocity of pure wave or current–wave flow whereas U_c is not influenced by wave motions, and is equal to the time-mean velocity of unidirectional flow passing a canopy. Representative velocity data of the total mimic canopy can be obtained by spatially averaging the data from the 4 locations in the mimic canopy (Fig. 1a).

Previous studies found that C_D was closely related to the Reynolds number (Re) [−] (reviewed in Nepf, 2011). In this study, it is defined using a characteristic velocity U_{max} [m/s]:

$$\mathrm{Re} = \frac{U_{\max} b_v}{\nu} \tag{4}$$

where $v = 10^{-6}$ m^2/s is the kinematic viscosity, U_{max} equals to the spatially averaged U_w for the pure wave conditions or spatially averaged $U_{mean} + U_w$ for current–wave conditions, respectively. Mendez et al. (1999) proposed a modified Reynolds number (Re*) [−], according to:

$$\mathrm{Re}^* = \frac{U^*_{\max} b_v}{v} \tag{5}$$

where U^*_{max} equals to the U_w in front of the tested canopy (x = 25 m in our experiments) at the top of the mimic stems.

2.2.2. C_D quantification by direct force measurement

Assuming the plant mimics are similar to an array of rigid piles, the Morison equation (Morison, 1950) can be applied to quantify the total force on them:

$$F = F_D + F_M = \frac{1}{2}\rho C_D h_v b_v u(t)|u(t)| + \frac{1}{4}\rho C_M \pi h_v b_v^2 \frac{\partial u(t)}{\partial t}. \tag{6}$$

where F_D is the drag force [N], F_M is the inertial force [N], ρ is fluid mass density [kg/m^3], h_v is the height of vegetation in water [m], b_v is the plant stem diameter [m] and C_D is the drag coefficient [−]. Furthermore, C_M is the inertia coefficient [−], equals to 2 for circular cylinders (Dean and Dalrymple, 1991). It is noted that F_M has no contribution to the WDV (Dalrymple et al., 1984). That is because the work performed by F_M per wave period equals zero. This holds for both pure wave and current–wave conditions. Hence, the work done by F_D in a wave period is equal to that done by F. Therefore, a period-averaged C_D can be obtained by quantifying the work done by F in a wave period. Hence:

$$C_D = \frac{2\int_{-\pi/\omega}^{\pi/\omega} F_D u dt}{\int_{-\pi/\omega}^{\pi/\omega} \rho h_v b_v u^2 |u| dt} = \frac{2\int_{-\pi/\omega}^{\pi/\omega} F u dt}{\int_{-\pi/\omega}^{\pi/\omega} \rho h_v b_v u^2 |u| dt}. \tag{7}$$

A space-averaged C_D can be derived by averaging the data from the 4 locations in the canopy (Fig. 1a).

2.3. Wave dissipation models

2.3.1. Wave dissipation model for pure wave cases

Applying the Morison equation and linear wave theory, Dalrymple et al. (1984) described monochromatic wave propagation in a plant canopy on a plain bed as:

$$K_v = \frac{H}{H_0} = \frac{1}{1+\beta D} \tag{8}$$

$$\beta = \frac{4}{9\pi} C_D b_v N H_0 k \frac{\sinh^3 k h_v + 3\sinh k h_v}{(\sinh 2kh + 2kh)\sinh kh} \tag{9}$$

where K_v is the relative wave height, H is the wave height [m] at distance D [m] in a canopy, H_0 is the wave height at the edge of the canopy, and k is the wave number [m^{-1}]. For pure wave cases, C_D is derived commonly by inverting Eq. (9), provided that β [m^{-1}] has been obtained by fitting Eq. (8) to measured WDV (e.g. Bradley and Houser, 2009; Jadhav et al., 2013).

To exclude the possible influence of bed and sidewall friction, the wave height reduction measured in the control tests (VD0) is subtracted from the one observed in the tests with mimic canopies (Augustin et al., 2009).

Wave height reduction per unit length of a plant canopy (ΔH) is derived as:

$$\Delta H = \frac{H_0 - H_{out}}{L} \tag{10}$$

where H_{out} is the wave height at the end of the mimic canopy [m] and L is the length of the canopy. To exclude the possible influence of bed and sidewall friction, the wave height reduction measured in the control tests (VD0) is subtracted from the one observed in the tests with mimic canopies (Augustin et al., 2009).

2.3.2. Analytical model for wave dissipation in current–wave flows

We propose a simple analytical model to better understand the effect of steady currents on WDV. This model is based on the following assumptions:

1) velocity u is uniform over the water depth;
2) turbulent velocity fluctuations (U' in Eq. (1)) are neglected;
3) the instantaneous horizontal orbital velocity is $U_w sin(\omega t)$;

4) for current–wave conditions, the period-averaged velocity equals the imposed current velocity, i.e. $U_{mean} = U_c$. Thus, the total instantaneous $u(t) = U_c + U_w sin(\omega t)$;
5) C_D and U_w do not vary when flow changes from pure wave conditions to current–wave conditions.

Based on the above assumptions, the period-averaged wave energy dissipation rate per unit area ε is expressed as follows.
For pure wave conditions:

$$\varepsilon_{pw} = \frac{\omega}{2\pi}\int_{-\pi/\omega}^{\pi/\omega} NF_D U_w \sin(\omega t)dt = \frac{\omega}{4\pi}\int_{-\pi/\omega}^{\pi/\omega} \rho C_D N b_v h_v |U_w \sin(\omega t)|(U_w \sin(\omega t))^2 dt = \frac{2}{3\pi}\rho C_D N b_v h_v U_w^3. \tag{11}$$

For current–wave conditions:

$$\begin{aligned}\varepsilon_{cw} &= \frac{\omega}{2\pi}\int_{-\pi/\omega}^{\pi/\omega} NF_D(U_c + U_w \sin(\omega t))dt = \frac{\omega}{4\pi}\int_{-\pi/\omega}^{\pi/\omega} \rho C_D N b_v h_v |U_c + U_w \sin(\omega t)|(U_c + U_w \sin(\omega t))^2 dt \\ &= \begin{cases} \frac{1}{2\pi}\rho C_D N b_v h_v [\sin^{-1}\left(\frac{|U_c|}{U_w}\right)\left(2|U_c|U_c^2 + 3|U_c|U_w^2\right) + \frac{1}{3}\left(4U_w^2 + 11U_c^2\right)\left(\sqrt{U_w^2 - U_c^2}\right)] & |U_c| < U_w \\ \frac{1}{4}\rho C_D N b_v h_v \left(2|U_c|U_c^2 + 3|U_c|U_w^2\right) & |U_c| \geq U_w \end{cases}.\end{aligned} \tag{12}$$

ε_{cw} is derived from the current–wave interaction, which can be divided into the wave induced energy dissipation rate ε_{cw_w} and the current induced energy dissipation rate ε_{cw_c} (Li and Yan, 2007):

$$\varepsilon_{cw_w} = \frac{1}{2}\rho C_D N b_v h_v |U_c| U_c^2. \tag{13}$$

Therefore, the ratio of ε_{cw_w} and ε_{pw} is:

$$f(\alpha) = \frac{\varepsilon_{cw_w}}{\varepsilon_{pw}} = \frac{\varepsilon_{cw} - \varepsilon_{cw\_c}}{\varepsilon_{pw}} = \begin{cases} \frac{3}{4}\sin^{-1}(|\alpha|)\left(2|\alpha|\alpha^2 + 3|\alpha|\right) + \frac{1}{4}\left(4 + 11\alpha^2\right)\sqrt{1-\alpha^2} - \frac{3\pi}{4}|\alpha|\alpha^2 & |\alpha| < 1 \\ \frac{9\pi}{8}|\alpha| & |\alpha| \geq 1 \end{cases}. \tag{14}$$

where $\alpha = U_c/U_w$. ε is proportional to the square of wave height. ΔH_{pw} is the reduced wave height per unit length of mimic canopies in pure wave conditions and ΔH_{cw} is that in current–wave conditions. Considering the different magnitudes of length scales, the relative wave height decay r_w can be derived as:

$$r_w = \frac{\Delta H_{cw}}{\Delta H_{pw}} = \sqrt{\frac{\varepsilon_{cw\_w}}{\varepsilon_{pw}}}. \tag{15}$$

However, our assumptions may be restrictive. Certain modifications may be necessary when applying this model for realistic conditions.

3. Results

3.1. Wave dissipation by mimic vegetation canopies

The measured K_v in pure wave conditions is shown in Fig. 3a. The tested canopies were VD2 and VD3. The tested wave condition was wave0410. With the same wave condition, a higher WDV was found in the mimic canopy with a higher mimic stem density and a lower submergence ratio. β can be derived by fitting Eq. (8) to the measured K_v. Subsequently, the obtained β can be substituted into Eq. (8) to describe the WDV (dashed line in Fig. 3a).

The effect of currents can be identified by comparing the WDV with different imposed current velocities (U_c) (Fig. 3b). The test shown in Fig. 3b was carried out in emergent conditions. The canopy stem density was VD3. Four steady currents, namely $U_c = 0$, 0.05 m/s, 0.15 m/s and 0.20 m/s, were imposed in combination with the same wave condition (wave0610). The corresponding α were 0, 0.6, 2.8 and 4.4, respectively. For the case with a relatively small α ($\alpha = 0.6$), the K_v along the canopy is higher than the one found in pure wave condition, thus a lower WDV. When the α is larger ($\alpha = 2.8$), the K_v is lower than that of the pure wave conditions, i.e. higher WDV. The WDV further increases when the α rises from 2.8 to 4.4.

The effect of the steady currents on WDV can be further evaluated by comparing the r_w. If it is larger than 1, it means that the WDV is increased with the presence of following currents. If it is less than 1, then WDV is reduced when following currents occur. The relation between the r_w and α is shown in Fig. 4. It shows that WDV in all the tests is influenced by following currents except the tests at the transition points, where the $r_w = 1$. Thus, the WDV is the same as it is in pure wave conditions. In different test conditions, transition points vary from 0.65 to 1.25. When the value of α is less than its value at the transition points, r_w is less than 1. Thus, the following currents decrease the WDV. In this range of α, r_w reaches its minimum when α is around 0.5. Subsequently, it starts increasing with α. When α exceeds the value at the transition points, $r_w > 1$. It means that in this range of α, the presence of currents increases the WDV. Therefore, the following currents can either increase or decrease WDV depending on α. Even though all the cases share the same general pattern, there are differences between the cases with different test conditions. Data from the VD1 canopy is more scattered than others. The minimum r_w ratios are lower in submerged canopies than that in emergent canopies.

Data obtained with comparable conditions in Paul et al. (2012) and Li and Yan (2007) are also plotted in Fig. 4. When the value of α is less than that at the transition point, our measurement result is similar to that of Paul et al. (2012), who evaluated the WDV with an α value

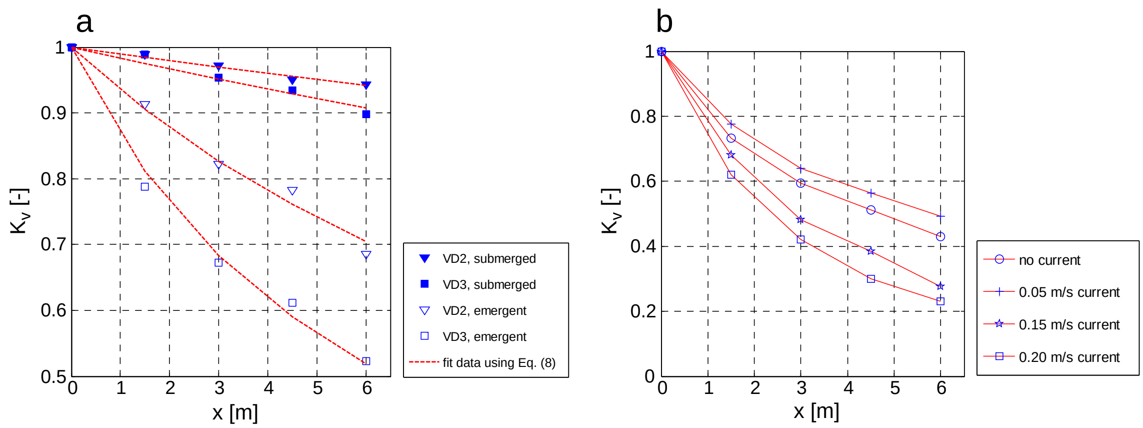

Fig. 3. Damping coefficient (K_v) evolution in mimic canopies. (a) The effect of mimic stem density and submergence ratio on K_v; (b) the effect of different imposing current velocities on K_v.

(0.47) lower than the transition point. However, when α is lower than the transition point, our result of r_w is less than the prediction of an empirical model in Li and Yan (2007). The model predicts that r_w is larger than 1 for all α (Fig. 4f). When α is high (>1.6), our measurement result is close to the experimental data and the model prediction of Li and Yan (2007). The equation describing the empirical model was not given in Li and Yan (2007), but its outcome was provided as a plot, which was adapted in Fig. 4f.

The prediction obtained with our analytical model (outlined in Section 2.3.2) is also plotted in Fig. 4f. Similar to the empirical model in Li and Yan (2007), the analytical model predicts that WDV increases monotonically with the velocity ratio α, which overestimates the WDV when α is small. To improve the model prediction, two modifications of the model are made:

1) the drag coefficient in current–wave cases is a proportion of that in pure wave cases, i.e. $C_{D\_cw} = 0.66 * C_{D\_pw}$. Such a ratio was derived from drag coefficient measurements (see Fig. 6).
2) in pure wave cases, the time-mean velocity (U_{mean}) is nonzero (see Fig. 7). U_{mean} is in the negative direction and $U_{mean}/U_w = -0.2$. Such a value is determined by averaging ratios measured in all the pure wave cases. In current–wave cases, U_{mean} is suppressed by wave motions (see Fig. 8). It is smaller than the imposed current velocity without wave influence (U_c) i.e. $U_{mean}/U_w - U_c/U_w = -0.2$. Such a value is determined by averaging the difference measured in all the current–wave cases.

With these two modifications, Eq. (14) can be rewritten as:

$$f'(\alpha) = \begin{cases} 1 & \alpha = 0 \\ 0.66\dfrac{f(\alpha - 0.2)}{f(-0.2)} & \alpha > 0 \end{cases}. \tag{16}$$

The result of this modification is shown in Fig. 4f. It appears that the modified analytical model is able to reproduce the general non-monotonic variation of r_w.

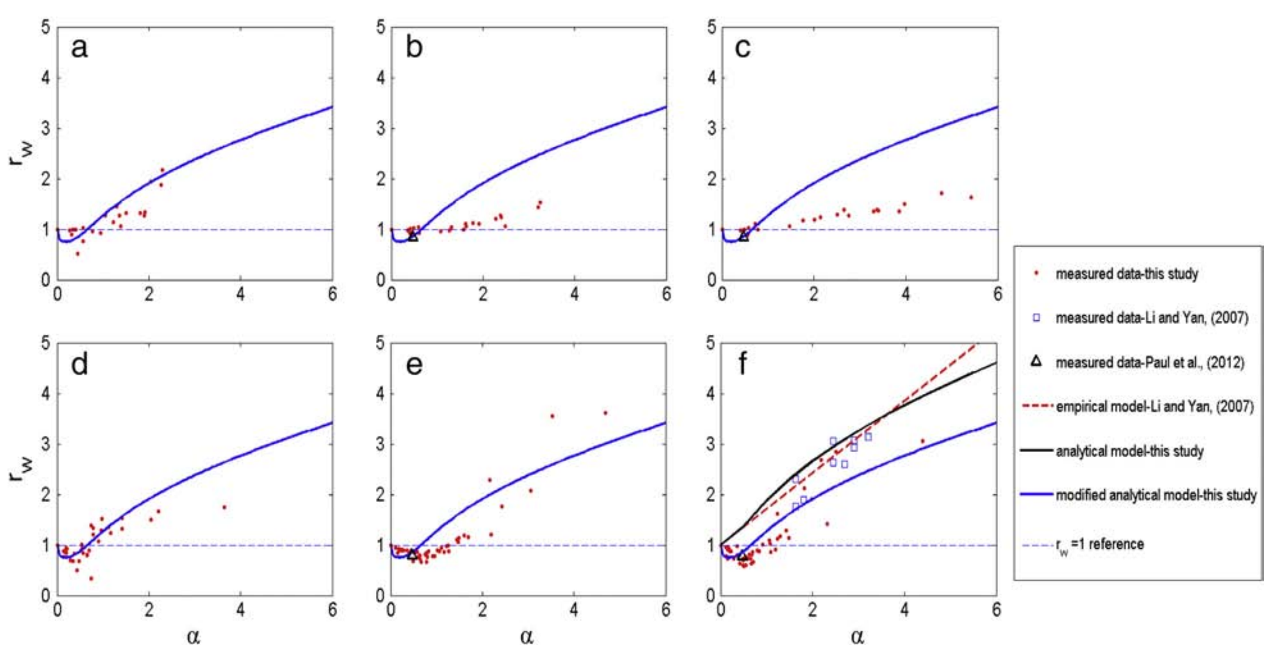

Fig. 4. Variation r_w with velocity ratios α. (a), (b), and (c) are emergent canopy with mimic stem densities VD1, VD2 and VD3, respectively; (d), (e), and (f) are submerged canopy with mimic stem densities VD1, VD2 and VD3, respectively.

3.2. Drag coefficient quantification

3.2.1. Time dependent drag force and drag coefficient

The time dependent F_D can be derived from in-phase data of F and u obtained at the same cross-sections of the flume (Eq. (6)). Fig. 5 shows the time-varying F and u at x = 29.5 m in the wave flume. The tests concern the submerged VD3 canopy in combination with the wave case wave1216. Fig. 5a and b shows that the measured oscillating u and F_D are generally in phase. The time lag between the two is very small (ca. 0.05 s). Fig. 5a further shows that u is asymmetric in the pure wave case. The period-averaged velocity (U_{mean}) is in negative direction. In the case with a small imposed current velocity ($U_c = 0.05$ m/s), the small U_c counteracts the period-averaged negative velocity and results in a more symmetric u, i.e. U_{mean} is close to zero. A larger U_c (0.15 m/s) can shift the overall u further towards the positive direction and results in a positive U_{mean}. The magnitudes of F_D with different following currents vary according to that of u (Fig. 5b).

Fig. 5c shows that the time dependent C_D varies with u and F_D accordingly. When u is near its crest or trough, the time-dependent C_D is relatively constant. However, when u is small, the time dependent C_D is unrealistically high because the velocity is approaching zero. It is also noted that the time dependent C_D can drop to zero when F_D is weak. Fig. 5c further demonstrates that the pure wave case is generally associated with a comparatively large C_D and an increase in U_c generally leads to a decrease of C_D.

3.2.2. Period-averaged drag coefficients

Previous study has indicated that the period-averaged C_D is closely related to the Reynolds number (reviewed in Nepf, 2011). Fig. 6 shows the relation between C_D and two Reynolds numbers, namely Re and Re*. These two Reynolds numbers are defined in Eqs. (4) and (5) respectively.

The C_D values presented in Fig. 6a are obtained in pure wave conditions by using the calibration approach (Eqs. (8) and (9)). Generally, C_D decreases with Re*, but the data points are scattered. The empirical relationship between C_D and Re* given by Mendez et al. (1999) is also plotted in Fig. 6a. Despite the scattering, the C_D obtained from the calibration approach is in the same range as estimated by the empirical relationship:

$$C_D = 0.08 + \left(\frac{2200}{\mathrm{Re}^*}\right)^{2.2} \qquad 200<\mathrm{Re}^*<15500. \tag{17}$$

Fig. 6b shows the C_D derived from the calibration approach as a function of Re. It is clear that the data is less scattered compared to that in Fig. 6a. The declining pattern of C_D with increasing Re is also more apparent. The C_D derived from emergent canopies is comparable to that from submerged canopies. It is noted that the submergence ratio has a minor effect on the variation of C_D with Re.

Fig. 6c shows the C_D values derived from the direct force measurements (Eq. (7)) for pure wave cases, as a function of Re. They were spatially averaged using 3 out of 4 locations that had simultaneous F and u measurements. FT2 failed during the experiment (see Fig. 1a) and it was excluded from the data analysis. It is clear that the derived C_D values share a similar decreasing pattern as that derived from the calibration approach. Specifically, when 300 < Re < 1000, the C_D drops quickly from around 4.0 to 1.7. When Re > 1000, the reduction of C_D with increasing Re becomes mild. Similar to the calibration approach, the submergence ratio hardly affects the C_D pattern. Emergent canopy cases generally had lower values of Re, which resulted in higher C_D values. Submerged canopy cases generally had higher values of Re, thus lower

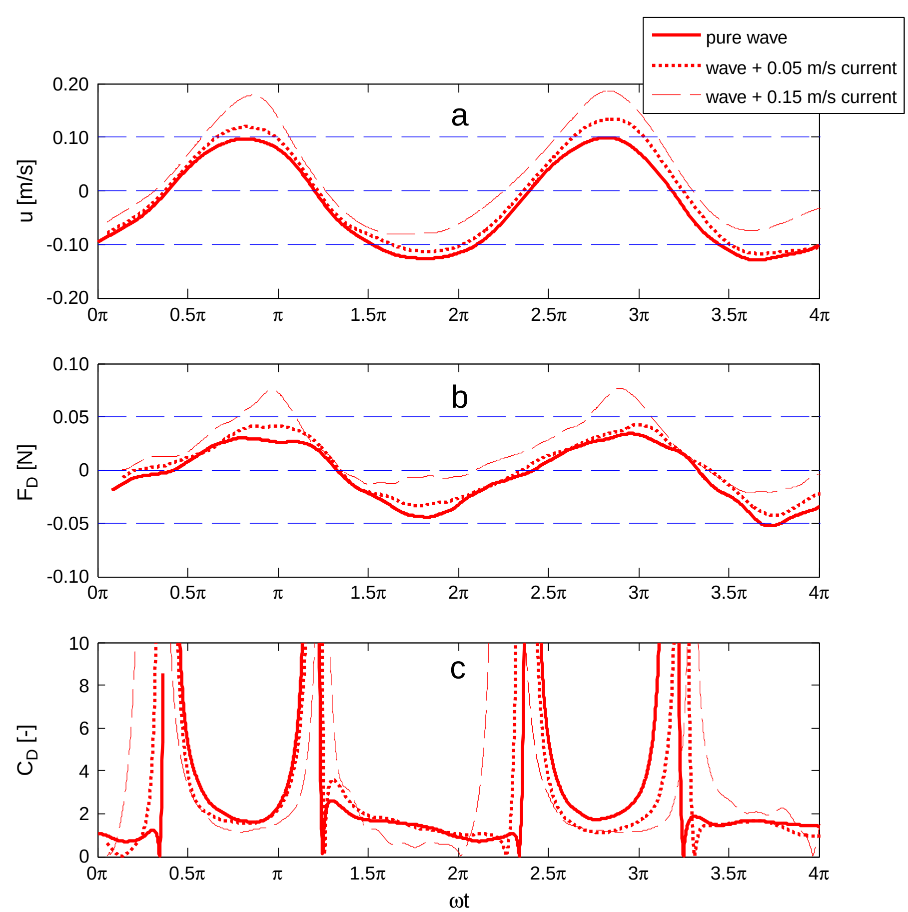

Fig. 5. Temporal variation of (a) velocity, (b) drag force and (c) drag coefficient with different imposed current velocities.

C_D values. It is evident that this direct measuring method leads to less scattering between C_D from different mimic stem densities.

The main advantage of applying the direct measuring approach is that it can be used to derive the C_D in current–wave flows. Fig. 6d presents the C_D values from both current–wave cases and pure wave cases (listed in Table 1). It shows that the typical decreasing pattern of C_D still holds in current–wave conditions. Compared to the pure wave cases, the current–wave cases were inherently associated with higher Re because of the superimposed current U_c. Consequently, the higher Re leads to lower C_D values in the current–wave cases. Particularly, when $600 < \mathrm{Re} < 1400$, the presence of currents can significantly decrease C_D. When $\mathrm{Re} > 1000$, however, for both pure wave and current–wave conditions the C_D value has a very gentle declining trend and the difference between the two conditions is small. In this range of Re, the mean C_D is 1.31 with a standard deviation of 0.22. Following the structure of the empirical relationship in Mendez et al. (1999), a relation between C_D and Re was found as the best fit ($R^2 = 0.89$) for all the data obtained from pure wave and current–wave cases (see Fig. 6d):

$$C_D = 1.04 + \left(\frac{730}{\mathrm{Re}}\right)^{1.37} \qquad 300<\mathrm{Re}<4700. \tag{18}$$

The tested Re in the pure wave case is in the range of 300–2800, while for current–wave tests it is 670–4700.

3.3. Velocity in canopies

3.3.1. Mean velocity profiles

Vertical profiles of mean velocity (U_{mean}) were measured in both emergent and submerged canopies. A U_{mean} that is representative for the entire mimic canopy is obtained by taking its average over the measuring locations at x = 27.5 m, 29.5 m and 30.5 m. The emergent (Fig. 7a) canopy was tested with case wave0612. The submerged canopy was tested with case wave1016 (Fig. 7b). The measured velocity profiles cover a major part of the water column ($z/h = 0.1$–0.7 for emergent canopy cases and $z/h = 0.1$–0.8 for submerged canopy cases). The other parts could not be measured as the EMF probes cannot be used close to the bed or above the wave trough. Fig. 7a shows that when the emergent canopy (VD1) is subjected to a pure wave flow, a negative U_{mean} exists throughout the measured depth. The variation along the vertical is small. The minimum U_{mean} is −0.014 m/s. A similar negative U_{mean} profile can be found in the control tests (VD0). In the pure current case, the U_{mean} profile in the control test (VD0) resembles a logarithmic profile. However, the presence of the mimic canopy (VD1) can significantly reduce the U_{mean} and result in a uniform profile. The comparison between current–wave and pure current cases suggests that the co-occurring waves suppress the imposed current velocity (U_c). Evidently, a lower U_{mean} can be found in the wave–current flows compared to that in pure current cases, with the maximum deficit being 0.021 m/s.

The results of the submerged canopy cases (Fig. 7b) are similar to the emergent canopy cases. The major difference is that a distinctive shear

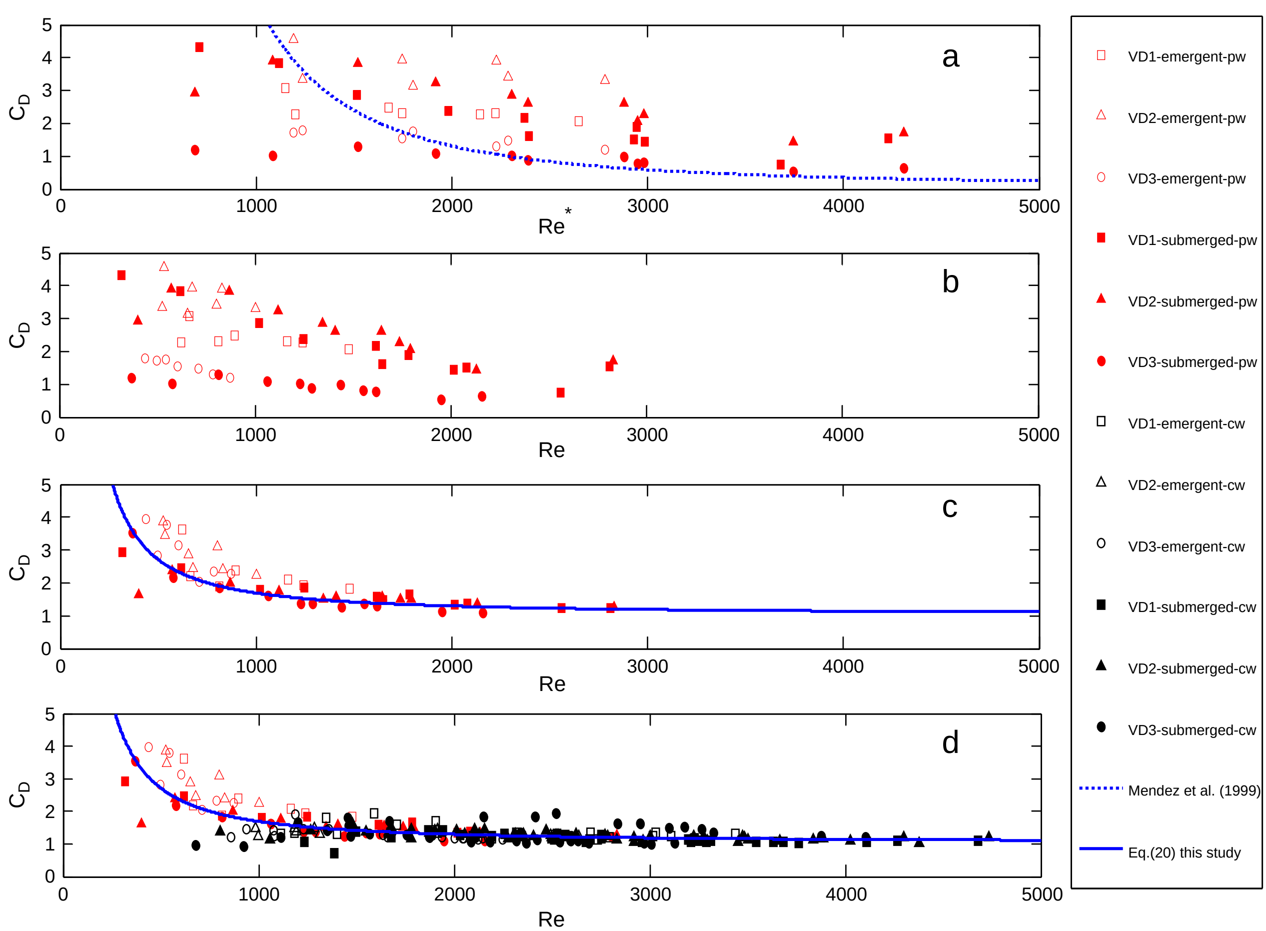

Fig. 6. Relation between Re and period-averaged C_D. (a) C_D in pure wave conditions derived by the calibration approach (using Eqs. (8) and (9)) as a function of Re*; (b) C_D in pure wave conditions derived by the calibration approach as a function of Re; (c) C_D in pure wave conditions derived by the direct force measurement approach as a function of Re; (d) C_D in pure wave and current–wave conditions derived by the direct force measurement approach as a function of Re; in the legend, 'pw' stands for pure wave conditions and 'cw' stands for current wave conditions.

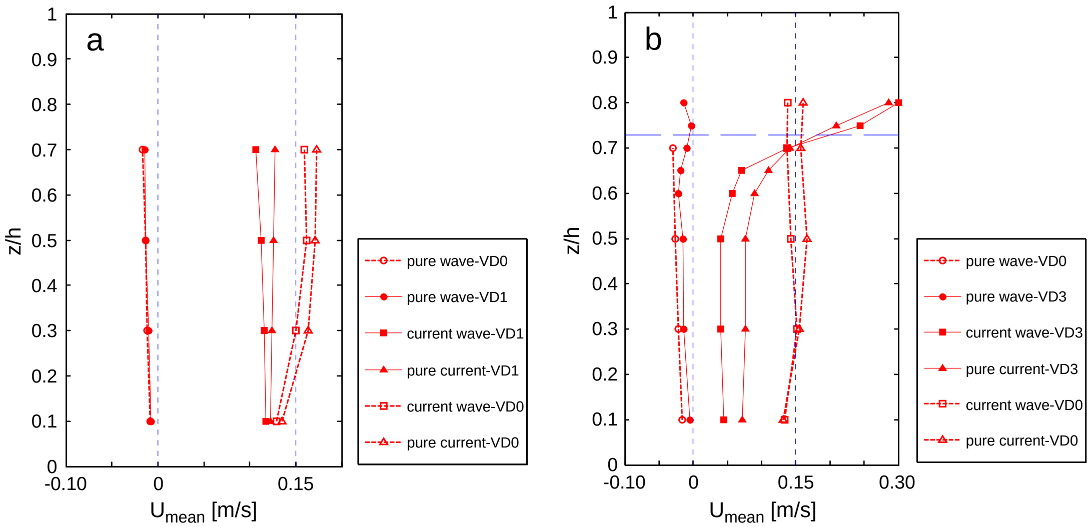

Fig. 7. Vertical profile of time-mean velocity (U_{mean}). (a) Emergent canopy; (b) submerged canopy, the horizontal dashed line indicates the relative height of the canopy. The dotted lines in each panel indicate the imposed U_c is 0 and 0.15 m/s, respectively.

layer exists near the canopy top when following currents exist. In pure wave conditions, a negative U_{mean} still can be found in the submerged canopy. A lower U_{mean} magnitude was also found in the current–wave case compared to that of a pure current case.

Fig. 8 compares U_{mean} with U_c. Both of them are nondimensionalized by U_w. For most data shown in Fig. 8, U_{mean}/U_w is smaller than U_c/U_w (i.e. α). It shows that wave motion has a tendency to form a negative velocity and suppress positive current velocities. In the submerged canopy case (Fig. 8b), when the flow is purely wave driven ($U_c/U_w = 0$), U_{mean} is in the negative direction so that U_{mean}/U_w is negative. When $0 < U_c/U_w < 0.35$, the negative U_{mean} is counteracted by the imposed positive currents and approaches zero. When $0.35 < U_c/U_w < 2.3$, U_{mean}/U_w shifts towards the positive direction but it is still smaller compared to U_c/U_w. When $2.3 < U_c/U_w$, the difference is negligible. The tests with the emergent canopy show a very similar pattern (Fig. 8a). However, the data from the emergent canopy is more equally distributed, whereas the data from the submerged canopy is mostly in a lower range of U_c/U_w.

4. Discussion

Our experimental results show that the effect of following currents on WDV does not vary monotonically with α but shows a decrease followed by an increase. A simple analytical model has been proposed to understand this mechanism. However, modifications to this model appeared necessary to capture the overall WDV variation. The reasons for these modifications lie in the assumptions made regarding drag coefficients and period-averaged velocities. The characteristics of the drag coefficient variation and in-canopy velocities dynamics are the key to understand the WDV variation with following currents.

4.1. Drag coefficients obtained by direct measurement approach

A commonly used method to obtain C_D is by calibrating WDV models (e.g. Eqs. (8) and (9)) against measured wave height decay. This method is prone to introducing modeling errors into the derived C_D. This

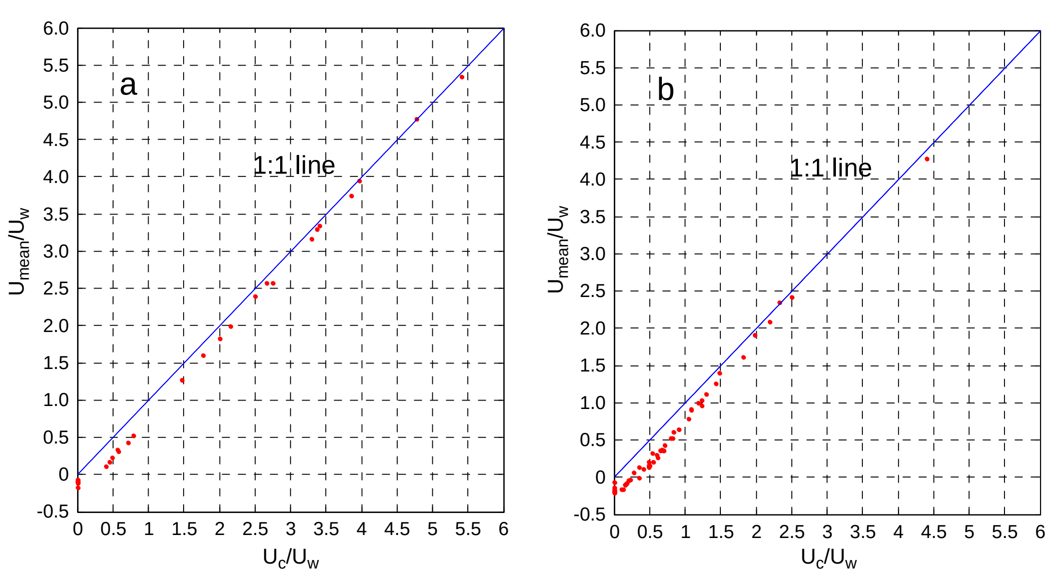

Fig. 8. Variation of the mean velocity (U_{mean}) with the imposed steady current velocity (U_c). (a) emergent canopy; (b) submerged canopy.

study applies a direct force measurement approach to derive the C_D, which eliminates the influence of modeling miscalculations. It is noted that even though C_D is derived from a different method, it stems from the original Morison equation and has the same definition as that derived from the calibration methods.

Since the measurement errors of the instruments are small (about 1%), the accuracy of this method mainly depends on the synchronization of the F and u data. Therefore, in our experiment, the force sensors and EMF were placed at same wave flume cross-sections. Still, a small time lag (ca. 0.05 s) exists in our measurements. This time lag may be induced by small misalignments between the EMF probes and force transducers and/or intrinsic delays of electronic instruments. As the time-dependent C_D is proportional to F_D/u^2, a small phase difference may lead to relatively large errors if u or F_D is close to zero (Fig. 5). In the major part of a wave period, the influence of this small time lag (0.05 s) is negligible as it is small compare to the tested wave period T (1.0 s–2.5 s). It is important to note that the work done by F_D is proportional to u^3 (Eqs. (12) and (13)). Thus, in a wave period, the work done by F_D when u equals zero is much less than that when u is near its peak. Therefore, in this study, the period-averaged C_D is obtained by integrating the work done by F_D in a wave period (Eq. (7)). This method automatically assigns less weight to the phase when u is near zero because of its small contribution to the WDV. This way, the obtained C_D is largely determined by the relatively high u and strong F_D in a wave period, which minimizes the influence of the time lag. Moreover, this method avoids the need for discriminating between F_D and F_M, which may also introduce errors in C_D.

The results show that C_D is negatively correlated to the Reynolds number, which agrees with previous studies (e.g. Augustin et al., 2009; Koftis et al., 2013). However, the Reynolds number Re is defined differently in the present study. In Mendez et al. (1999), the Reynolds number Re* was defined by using U_w in front of the canopy as the characteristic velocity (Eq. (5)). However, it is apparent that wave height decreases along plant canopies and U_w decreases accordingly. The Re* only takes into account the U_w in front of the canopy, which is not representative of the hydrodynamic conditions inside a canopy, especially when the WDV is high. This may explain the large scatter when C_D is plotted against Re* (Fig. 6a). In our study, Re is defined using the measured in-canopy velocity U_{max} as the characteristic velocity (Eq. (4)). U_{max} directly interacts with plant mimics, which is more representative for the hydrodynamic conditions inside a canopy.

When comparing the two different methods of deriving C_D (calibration approach and direct force measurement, presented in Fig. 6b and c, respectively), it can be seen that the scatter of C_D is larger between different mimic stem densities following the calibration method. The reason for this may be that the calibration approach assumes that u in a canopy follows the linear wave theory and is not attenuated by the plant stems. In reality, however, u is reduced due to the presence of plant stems and this reduction varies with the plant stem density (Pujol et al., 2013; Stratigaki et al., 2011). The calibration approach neglects such a variation and attributes it solely to C_D, which leads to scattered C_D between different densities. The direct measuring method, on the other hand, collects the in-canopy u data. The variation induced by vegetation density is inherently considered, which results in less spreading of C_D (Fig. 6c). It is worth noticing that the tested Re in our experiments is 300–4700 and the frontal area per canopy volume is 0.62 m^{-1}, 1.39 m^{-1} and 5.56 m^{-1} for three different mimic stem densities. The dependence of C_D on the mimic stem density is found to be weak in such conditions. With a different range of Re or mimic stem densities, the dependence can be stronger as found in previous studies (Huang et al., 2011; Tanino and Nepf, 2008).

Notably, the direct force measuring technique enables us to obtain the C_D in current–wave flows, which is not possible with the calibration method. To our knowledge, the C_D of mimic vegetation canopies in current–wave flows has not been assessed previously. Our results show that C_D values in current–wave conditions follow the same decreasing pattern as in pure wave conditions. In general, the presence of a current decreases the C_D since the Re is increased. This finding is consistent with the observation in tests with an isolated cylinder (Sumer and Fredsøe, 2006; Zhou and Graham, 2000). Zhou and Graham (2000) explained that the reduction of C_D was because the vortex formation, shedding and oscillatory motion in pure wave conditions were altered by the imposed steady currents. In pure wave conditions, the vortices act at both the downstream and upstream sides of a stem. When steady currents are present, the vortices are shifted to the downstream side. This results in less obstruction 'seen' by water particles, namely less drag of the flow. To include this phenomenon, we propose an overall empirical relation of C_D for both pure wave and current–wave conditions (Eq. (18)). Such a relation can be useful in understanding WDV and predicting it in numerical modeling studies. For example, if Re > 1000 in a test case, $C_D = 1.31$ can be a reasonable first estimate. In detailed spectral wave models or phase-resolving models, Re in a canopy can be easily accessed and the value of C_D can be estimated from this relation subsequently.

4.2. Wave dissipation in pure wave and current–wave flows

Test results obtained in pure wave conditions show that WDV is higher when the mimic canopies have a higher N and a lower submergence ratio (Fig. 3a), which is consistent with previous studies (e.g. Mendez and Losada, 2004; Paul et al., 2012; Stratigaki et al., 2011). The main objective of this study, however, is to understand the effect of following currents on WDV, on which the previous two studies have drawn contradicting conclusions (Li and Yan, 2007; Paul et al., 2012). Our study shows that when α is small, following currents generally reduce the WDV. However, when α is sufficiently large, currents can also promote the WDV (Fig. 4). Hence, it depends on α whether following currents suppress or intensify WDV. The two previous studies investigated WDV in different ranges of α, which caused the seeming inconsistency.

Li and Yan (2007) predicted WDV to increase linearly with the velocity of following currents and such a rise was attributed to wave–current interactions. However, our measured data shows that WDV is only enhanced when α is larger than the corresponding transition points, which are in the range 0.65–1.25 depending on the tested canopy (Fig. 4). The α tested in the physical experiments of Li and Yan (2007) were all above 1.5. Therefore, WDV reduction by following currents (i.e. $r_w < 1$) in low α was not observed by them. On the other hand, Paul et al. (2012) measured WDV with low α (<0.5) and concluded that WDV was reduced in current–wave flow. In our experiment, WDV is only reduced when α is less than its value at the transition points (Fig. 4).

The variation of U_{mean} with α is also important in understanding the tendencies of WDV. In pure wave conditions, a negative U_{mean} exists in pure wave conditions, which can be explained by the Stokes wave theory (Pujol et al., 2013). Above the wave trough level, the U_{mean} is in the positive direction. In a wave flume with closed boundaries, there must be zero net transport. Hence, below the wave trough level a net negative U_{mean} must exist to compensate for the positive flux above. In pure wave conditions, the non-zero U_{mean} leads to a higher WDV compared to that with idealized velocity symmetry because of the current–wave interaction (Eq. (14)). When a small positive U_c is imposed, it counteracts the negative U_{mean} and forces the overall velocity to be symmetric (Fig. 5a). The magnitude of U_{mean} is then reduced to zero, which results in a lower WDV (Eq. (14)). As the imposed U_c increases, U_{mean} shifts into the positive direction and starts increasing its magnitude again, which promotes WDV and eventually leads to a higher WDV than that in the pure wave conditions.

The variation of C_D is also closely related to the tendencies of WDV with α. In Fig. 8b, U_{mean} reaches zero when α is around 0.35. When $0.35 < \alpha < 0.5$, U_{mean} is in the positive direction and its magnitude is increasing with α. However, WDV (i.e. r_w in Fig. 4f) does not reach its minimum when U_{mean} reaches zero (i.e. $\alpha = 0.35$). It keeps decreasing until it reaches its minimum when $\alpha \approx 0.50$. The further reduction of WDV is induced by the continuous decline of C_D (Fig. 6d). Hence, the tendencies of WDV are influenced by the combined effects of U_{mean} and C_D variation. By adapting the variation of U_{mean} and C_D with α, the modified model is capable of describing the non-monotonic dynamics of WDV (Fig. 4f).

Paul et al. (2012) explained the reduction of WDV in current–wave flows by the bending of the non-rigid mimics, which reduces the drag-forming area of the canopy. However, our study used rigid wooden rods as plant mimics, which deform negligibly with the water motion. Nevertheless, the reduction in WDV can still be found when α is small. Hence, such a reduction is not necessarily induced by canopy deformation. The decrease of WDV can also be induced by the reduction of C_D and the magnitude of U_{mean} (Figs. 6 and 8). It is possible that these two factors also played a role in the observed WDV decline in flexible canopies.

Natural salt marsh and mangrove wetlands are often bounded by sea dikes on their landward side. The dikes are closed boundaries similar to those in confined flumes. Thus, the above-motioned interactions between the wave-induced velocities and tidal currents may also take place in real coastal wetlands. This study shows that the wave dissipation capacity of a certain plant canopy can be reduced as much as 50% when α is around 0.5. During storm events, U_w can be significantly larger than current velocities during a regular flood, which leads to very low α values. As a consequence, the WDV can be significantly reduced in such a scenario. It is important to take into account the possible negative effect of flooding currents on WDV when integrating natural wetlands into coastal protection schemes.

5. Conclusions

This study primarily evaluated the effect of following currents on WDV by flume experiments. An analytic model was built to understand such effect. It was observed that following currents can affect WDV in all the tested canopies with different mimic stem density and submergence ratio. The effect of following currents on WDV can be either suppressing or promoting, which depends on the ratio between current velocity and the amplitude of horizontal orbital velocity (α). When α is small, WDV is reduced owing to the reduction of C_D and U_{mean} magnitude. When α is sufficiently high, WDV can be strengthened due to current–wave interaction. These observations can explain the contradictive conclusions in the previous studies that investigated WDV in different ranges of α (Li and Yan, 2007; Paul et al., 2012). Our findings suggest that the flooding tide during storm events could be a critical scenario for coastal protection schemes that utilize coastal wetlands to attenuate wave energy. In order to understand WDV, a direct force measurement approach was applied to derive drag coefficient C_D. This method can be applied to obtain the C_D in current–wave flows, which has not been assessed previously. An empirical relation between drag coefficient and Re has been formulated based on the measured data. This relation can be useful for future studies on wave–current–vegetation interaction.

Acknowledgments

The first author (Z. Hu) is supported by the China Scholarship Council (grant number: 2010671012). We acknowledge Dr. Tjeerd Bouma for offering the force transducers, Dr. Maike Paul for providing data of the previous study, Dr. Jasper Dijkstra for giving writing advice and Drs. Mariette van Tilburg for editing the manuscript. We also thank Mr. Sander de Vree, Mr. Jaap van Duin, Mr. Yan Ni, Ms. Mirjam Flierman and Ms. Lora Buckman for assisting with construction and measurements in the wave flume.

References

Anderson, M.E., Smith, J.M., McKay, S.K., 2011. Wave dissipation by vegetation. Coastal and Hydraulics Engineering Technical Note ERDC/CHL CHETN-I-82. U.S. Army Engineer Research and Development Center, Vicksburg, MS.

Augustin, L.N., Irish, J.L., Lynett, P., 2009. Laboratory and numerical studies of wave damping by emergent and near-emergent wetland vegetation. Coast. Eng. 56, 332–340.

Borsje, B.W., van Wesenbeeck, B.K., Dekker, F., Paalvast, P., Bouma, T.J., van Katwijk, M.M., de Vries, M.B., 2011. How ecological engineering can serve in coastal protection. Ecol. Eng. 37, 113–122.

Bouma, T.J., De Vries, M.B., Low, E., Peralta, G., Tánczos, I.C., Van De Koppel, J., Herman, P.M.J., 2005. Trade-offs related to ecosystem engineering: a case study on stiffness of emerging macrophytes. Ecology 86, 2187–2199.

Bradley, K., Houser, C., 2009. Relative velocity of seagrass blades: implications for wave attenuation in low-energy environments. J. Geophys. Res. Earth Surf. 114.

Callaghan, D.P., Bouma, T.J., Klaassen, P., van der Wal, D., Stive, M.J.F., Herman, P.M.J., 2010. Hydrodynamic forcing on salt-marsh development: distinguishing the relative importance of waves and tidal flows. Estuar. Coast. Shelf Sci. 89, 73–88.

Dalrymple, R.A., Kirby, J.T., Hwang, P.A., 1984. Wave diffraction due to areas of energy dissipation. J. Waterw. Port Coast. Ocean Eng. 110, 67–79.

Dean, R., Dalrymple, R., 1991. Water wave mechanics for engineers and scientists. Adv. Ser. Ocean Eng., vol. 2. World Scientific, Tokyo.

Delft Hydraulics, 1990. User's manual for the delft hydraulics four quadrant electromagnetic liquid velocity meter. 5.

Delft Hydraulics, year unknown. Manual for Wave Height Meter. p. 2.

Demirbilek, Z., Dalrymple, R.A., Sorenson, R.M., Thompson, E.F., Weggel, J.R., 1996. Water waves. In: Heggen, R.J. (Ed.), Hydrology Handbook. ASCE, New York, pp. 627–720.

Huang, Z., Yao, Y., Sim, S.Y., Yao, Y., 2011. Interaction of solitary waves with emergent, rigid vegetation. Ocean Eng. 38, 1080–1088.

Infantes, E., Orfila, A., Bouma, T.J., Simarro, G., Terrados, J., 2011. *Posidonia oceanica* and *Cymodocea nodosa* seedling tolerance to wave exposure. Limnol. Oceanogr. 56, 2223–2232.

Jadhav, R.S., Chen, Q., Smith, J.M., 2013. Spectral distribution of wave energy dissipation by salt marsh vegetation. Coast. Eng. 77, 99–107.

Koftis, T., Prinos, P., Stratigaki, V., 2013. Wave damping over artificial *Posidonia oceanica* meadow: a large-scale experimental study. Coast. Eng. 73, 71–83.

Li, C.W., Yan, K., 2007. Numerical investigation of wave–current–vegetation interaction. J. Hydraul. Eng. 133, 794–803.

Lowe, R.J., Koseff, J.R., Monismith, S.G., 2005. Oscillatory flow through submerged canopies: 1. Velocity structure. J. Geophys. Res. C: Oceans Atmos. 110, 1–17.

Lowe, R.J., Falter, J.L., Koseff, J.R., Monismith, S.G., Atkinson, M.J., 2007. Spectral wave flow attenuation within submerged canopies: implications for wave energy dissipation. J. Geophys. Res. C: Oceans Atmos. 112.

Luhar, M., Coutu, S., Infantes, E., Fox, S., Nepf, H., 2010. Wave-induced velocities inside a model seagrass bed. J. Geophys. Res. C: Oceans Atmos. 115.

Mendez, F.J., Losada, I.J., 2004. An empirical model to estimate the propagation of random breaking and nonbreaking waves over vegetation fields. Coast. Eng. 51, 103–118.

Mendez, F.J., Losada, I.J., Losada, M.A., 1999. Hydrodynamics induced by wind waves in a vegetation field. J. Geophys. Res. C: Oceans Atmos. 104, 18383–18396.

Möller, I., 2006. Quantifying saltmarsh vegetation and its effect on wave height dissipation: results from a UK East coast saltmarsh. Estuar. Coast. Shelf Sci. 69, 337–351.

Morison, J.R., 1950. The force exerted by surface waves on piles. Pet. Trans. AWME 189.

Nepf, H.M., 2011. Flow over and through biota. In: Wolanski, E., McLusky, D. (Eds.), Treatise on Estuarine and Coastal Science. Academic Press, Waltham, pp. 267–288.

Paul, M., Bouma, T.J., Amos, C.L., 2012. Wave attenuation by submerged vegetation: combining the effect of organism traits and tidal current. Mar. Ecol. Prog. Ser. 444, 31–41.

Pujol, D., Serra, T., Colomer, J., Casamitjana, X., 2013. Flow structure in canopy models dominated by progressive waves. J. Hydrol. 486, 281–292.

Shi, B.W., Yang, S.L., Wang, Y.P., Bouma, T.J., Zhu, Q., 2012. Relating accretion and erosion at an exposed tidal wetland to the bottom shear stress of combined current–wave action. Geomorphology 138, 380–389.

Stratigaki, V., Manca, E., Prinos, P., Losada, I.J., Lara, J.L., Sclavo, M., Amos, C.L., Cáceres, I., Sánchez-Arcilla, A., 2011. Large-scale experiments on wave propagation over *Posidonia oceanica*. J. Hydraul. Res. 49, 31–43.

Sumer, B.M., Fredsøe, J., 2006. Advanced Series on Ocean Engineering, Volume 12: Hydrodynamics around Cylindrical Structures, revised ed. World Scientific Pub., London 157–160.

Suzuki, T., Zijlema, M., Burger, B., Meijer, M.C., Narayan, S., 2011. Wave dissipation by vegetation with layer schematization in SWAN. Coast. Eng. 59, 64–71.

Tanino, Y., Nepf, H.M., 2008. Laboratory investigation of mean drag in a random array of rigid, emergent cylinders. J. Hydraul. Eng. 134, 34–41.

Yang, S.L., Shi, B.W., Bouma, T.J., Ysebaert, T., Luo, X.X., 2012. Wave attenuation at a salt marsh margin: a case study of an exposed coast on the Yangtze Estuary. Estuar. Coasts 35, 169–182.

Ysebaert, T., Yang, S.L., Zhang, L., He, Q., Bouma, T.J., Herman, P.M.J., 2011. Wave attenuation by two contrasting ecosystem engineering salt marsh macrophytes in the intertidal pioneer zone. Wetlands 31, 1043–1054.

Zhou, C.Y., Graham, J.M.R., 2000. A numerical study of cylinders in waves and currents. J. Fluids Struct. 14, 403–428.